Accelerating materials discovery by high-throughput GIWAXS characterization of quasi-2D formamidinium metal halide perovskites

Jonghee Yang[1], Juanita Hidalgo[2], Sergei V. Kalinin[1], Juan-Pablo Correa-Baena[2], Mahshid Ahmadi[1]*

[1] *Institute for Advanced Materials and Manufacturing, Department of Materials Science and Engineering, University of Tennessee, Knoxville, TN 37996, United States*

[2] *School of Materials Science and Engineering, Georgia Institute of Technology, Atlanta, GA 30332, United States*

*E-mail: mahmadi3@utk.edu

Abstract

The intriguing functionalities of emerging quasi-two-dimensional (2D) metal halide perovskites (MHPs) have led to further exploration of this material class for sustainable and scalable optoelectronic applications. However, the chemical complexities in precursors – primarily determined by the 2D:3D compositional ratio – result in uncontrolled phase heterogeneities in these materials, which compromises the optoelectronic performances. Yet, this phenomenon remains poorly understood due to the massive quasi-2D compositional space. To systematically explore the fundamental principles, herein, a high-throughput automated synthesis-characterization workflow is designed and implemented to formamidinium (FA)-based quasi-2D MHP system. It is revealed that the stable 3D-like phases, where the α-$FAPbI_3$ surface is passivated by 2D spacer molecules, exclusively emerge at the compositional range (35-55% of $FAPbI_3$), deviating from the stoichiometric considerations. A quantitative crystallographic study via high-throughput grazing-incidence wide-angle X-ray scattering (GIWAXS) experiments integrated with automated peak analysis function quickly reveals that the 3D-like phases are vertically aligned, facilitating vertical charge conduction that could be beneficial for optoelectronic applications. Together, this study uncovers the optimal 2D:3D compositional range for complex quasi-2D MHP systems, realizing desired optoelectronic performances and stability. The automated experimental workflow significantly accelerates materials discoveries and processing optimizations while providing fundamental insights into complex materials systems.

Introduction

Metal halide perovskites (MHPs) have gained extensive attention as materials platform for next-generation optoelectronic applications including photovoltaics (PVs), light-emitting devices (LEDs), and neuromorphic electronics.[1-5] This is attributed to their excellent materials properties realizing high optoelectronic performances and facile solution processibility suited to scalable productions.[6] Nevertheless, one of the crucial bottlenecks retarding the ubiquitous applications of the MHPs in the real world is poor stability. The lability of the materials readily causes significant losses of the outstanding functionalities, which in turn become no longer suited to long-term sustainable applications.[7-9]

Quasi-two-dimensional (2D) MHPs have recently emerged as a promising materials class that shows significantly enhanced stability than three-dimensional (3D) analogues.[10] Quasi-2D MHPs exhibit unique crystallographic structures that differentiate them from their 3D counterparts, where the large-sized organic cations, called spacers, confine the MHP crystal structure at the surface to be grown along 2D space.[11, 12] This enables tuning of optoelectronic characteristics by thickness control of the confined structure – quantified by the number of the MHP monolayer (n) in the confined structure; it can be described as a chemical formula of $L_2A_{n-1}B_nX_{3n+1}$ (L, A, B and X are monovalent spacer cations, monovalent organic/inorganic cations, divalent metal cations and halides, respectively).[11, 12] Additionally, the spacer cation can protect the functional phase structure against deformation via external stresses, thereby enhancing the phase stability compared to the 3D MHP counterparts – particularly, $FAPbI_3$-based systems.[10, 13]

While the phase stability problem is significantly mitigated, still the optoelectronic performances of the quasi-2D MHP systems, particularly in PV applications, are lagging behind that of 3D.[14, 15] This is attributed to the uncontrolled emergence of multiple quasi-2D phases in the films,[16] where such phase heterogeneity significantly compromises the carrier conduction properties.[17, 18] In some specific cases, the phase heterogeneity in quasi-2D MHPs can be evolved along the vertical direction of the films – 3D-rich at the top, 2D-rich at the bottom of the MHP films,[19, 20] attributed to the imbalanced crystallization kinetics of 3D and 2D MHP components.[21]

In fact, the crystallization of quasi-2D MHPs – a chemically complex materials system – is largely dependent on multiple physio-chemical factors.[20, 22-27] Particularly, the ratio of 2D:3D

compositions in the MHP precursors primarily influences the final phase constitution of the quasi-2D MHP films.[21] Notwithstanding, so far, there is no consensus or fundamental guidelines for designing an optimal 2D:3D composition ratio within a wide range of MHP compositional space exhibiting best optoelectronic performances. In fact, most publications demonstrating high-performance quasi-2D MHP optoelectronics have utilized various 2D:3D composition ratios, each of which strongly stems from the preliminary optimization process of each research group, but with a handful of basis sets.[16, 28-30] Such inconsistency is now crucially decelerating the lab-to-fab transformation and realization of scalable manufacturing quasi-2D MHP optoelectronics in the real world.

Herein, we implement a high-throughput automated experimental workflow to systematically explore the phase heterogeneity of quasi-2D MHPs as a function of 2D:3D compositional ratios.[21, 31] By using a robotic pipetting platform, an array of 96 quasi-2D MHP films are quickly synthesized, and the phase distributions and their time-evolutions in each film – along the vertical directions and compositional changes – are autonomously characterized via photoluminescence (PL) spectroscopy. A machine learning (ML)-based analysis effectively reveals the compositional and geometric constitutions of the associated phases in the system from the massive PL dataset, the amount of which is impossible for individual to manually analyze.

In this study, we specifically selected the phenethylammonium (PEA) and formamidinium (FA)-based quasi-2D MHP system, which shows promising functionalities although suffering from thermodynamic instability of functional α-$FAPbI_3$ phase that causes phase heterogeneities.[1, 13, 23, 26, 32, 33] We observe that 3D-like phases, α-$FAPbI_3$ MHPs where the phase stability is enhanced by surface passivation of PEA cations,[10] exclusively emerge in the 2D:3D compositional space of 35-55% of $FAPbI_3$ ratio. Note that this compositional range far deviates from the stoichiometric considerations, which is difficult to manually predict by chemical intuitions based on the handful of experiments.[13, 24]

We further explore the evolutions of crystallographic structures and orientations of the MHP phases in the quasi-2D compositional space via high-throughput grazing-incidence wide-angle X-ray scattering (GIWAXS) experiments, allowing comprehensive structural understandings of the functional materials system. Here, an automated peak analysis function is implemented for analyzing 285 individual GIWAXS patterns,[21] not only accelerating the overall materials discovery sequence but also uncovering the global trends of phase constitutions, vertical

distributions and, orientations in the complex system. Our analysis revealed that vertically aligned α-$FAPbI_3$ MHPs emerge at the compositional range exactly where the PL of the stable 3D-like phases is observed. The joint high-throughput explorations of quasi-2D MHPs clearly uncovers the optimal 2D:3D ratios for desired functionalities with structural insights, thereby providing a guideline required for design of functional systems.

Our study exemplifies how a high-throughput synthesis-characterization workflow can effectively accelerate the discoveries of complex material systems exhibiting multiple functionalities and the sequence of processing optimizations. Moreover, these findings provide comprehensive insights into the fundamental principles controlling the phase constitutions in the quasi-2D MHPs, which is vital for designing functional systems that can be directly implemented in the scalable manufacturing processes.

Results and Discussion

Various studies have explored the crystallization behavior and the resulting phase distributions in quasi-2D MHP systems, revealing that multiple parameters and factors, including solvent-solute interactions, crystallization rates, ion diffusion behaviors and temperatures, can sensitively affect the resulting system.[20, 22-27] Among them, the most intuitive determinant controlling the final phase distributions of quasi-2D MHPs is the ratio of 2D:3D compositions.[21] Nevertheless, there is not a united, generalized principles on how to design the quasi-2D MHP system with an optimal 2D:3D ratio for high-performance MHP optoelectronics, even though many publications have already demonstrated excellent device performances. In fact, the exploration of the optimal 2D:3D concentration of MHP from the massive quasi-2D compositional space through the classical batch-type experiments requires intensive efforts at the expense of tremendous time and energy.

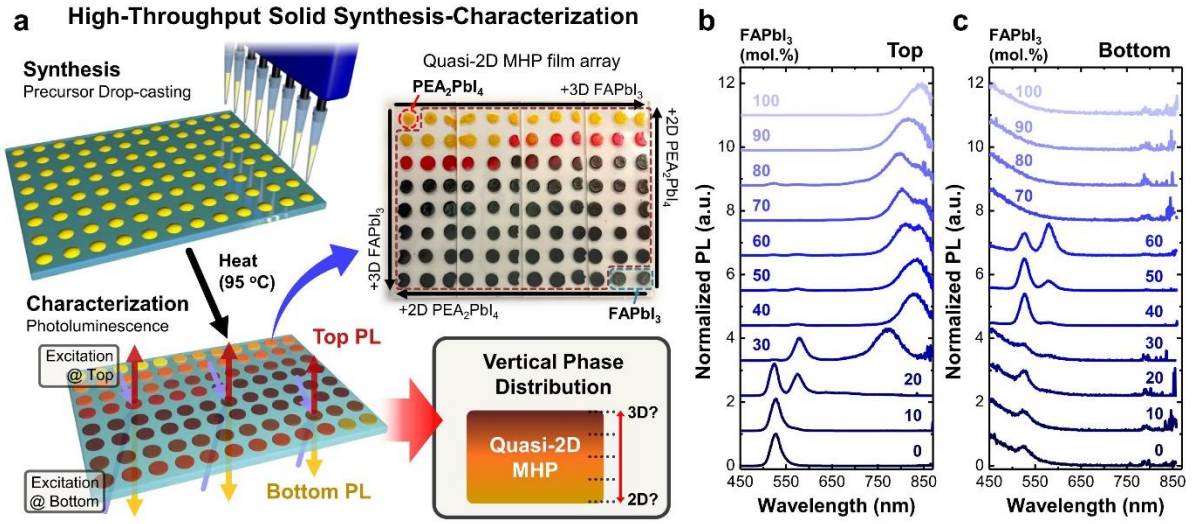

Fig. 1. a, Schematics describing high-throughput synthesis and characterization of drop-casted PEA-FA quasi-2D MHP array. By using a fast-response optical reader, the PL spectra of top- and bottom-side of the films are collected as function of time, providing comprehensive insights into compositional and geometric phase distributions with corresponding phase stability of the film system. **b** and **c**, Representative top- and bottom-oriented initial PL spectra of the drop-casted quasi-2D MHP films with different 2D:3D composition ratios.

Here we implement a high-throughput automated synthesis-characterization workflow based on a robotic pipetting platform to explore the quasi-2D MHP film system.[21, 34, 35] First, a series of quasi-2D precursor solutions with 95 different 2D:3D MHP ratios in the compositional space is prepared by accurately mixing both 2D and 3D solutions with a designed volume ratio (2D:3D) in each well of a microplate. By using an 8-channel pipet, the precursor solutions are drop-casted onto the glass substrates and subsequently heated (at 95 ^{o}C for 10 min) under an N_2 atmosphere (**Supplementary Fig. 1**). As a result, an array of quasi-2D MHP films with 95 different 2D:3D compositions are fabricated.[36, 37] The deposition and annealing process takes only 2 hours in total and thus, significantly accelerates the fabrication sequence. The as-prepared MHP array is quickly transferred to an optical reader, where the PL spectra are collected from both the top and bottom sides of each film for 26 hours (**Supplementary Fig. 2 and 3**). This allows us to understand the general trend of phase distributions not only in the 2D:3D MHP compositional space but also in the vertical direction of each MHP film (**Fig. 1a**).[20, 38] From initial PL spectra, the n=1 and 2 phases of 2D MHPs are dominant. This trend continues up to the $FAPbI_3$ ratio of ~30%, where the emission from higher-n 2D phases (n≥5; peak wavelength >750 nm) and 3D $FAPbI_3$ MHPs (peak wavelength ~820 nm) gradually

emerge and become dominant by further increasing the $FAPbI_3$ ratios (**Fig. 1b**).[21, 39] Note that, up to the $FAPbI_3$ ratio of ~80%, the emergences of higher-*n* MHPs also involve the *n*=1 and/or 2 phases, as evidenced by the corresponding PL at ~525 and ~580 nm, respectively (**Supplementary Fig. 4**). This could be attributed to the disproportionation of intermediate phases (i.e., *n*=3 and 4) and/or preferential formation in the crystallization process.[21, 23] In contrast, only the *n*=1 and 2 phases are observed from the bottom of the films, particularly up to 60% $FAPbI_3$ ratio (**Fig. 1c**). Such a phase heterogeneity in the vertical direction has been explained by the surface-initiated MHP crystallization behavior; the 3D and higher-*n* MHP phases are first crystallized on the top of the precursor droplet (i.e., liquid-air interface) and the remaining 2D precursors are lastly crystallized on the bottom.[19, 20, 38]

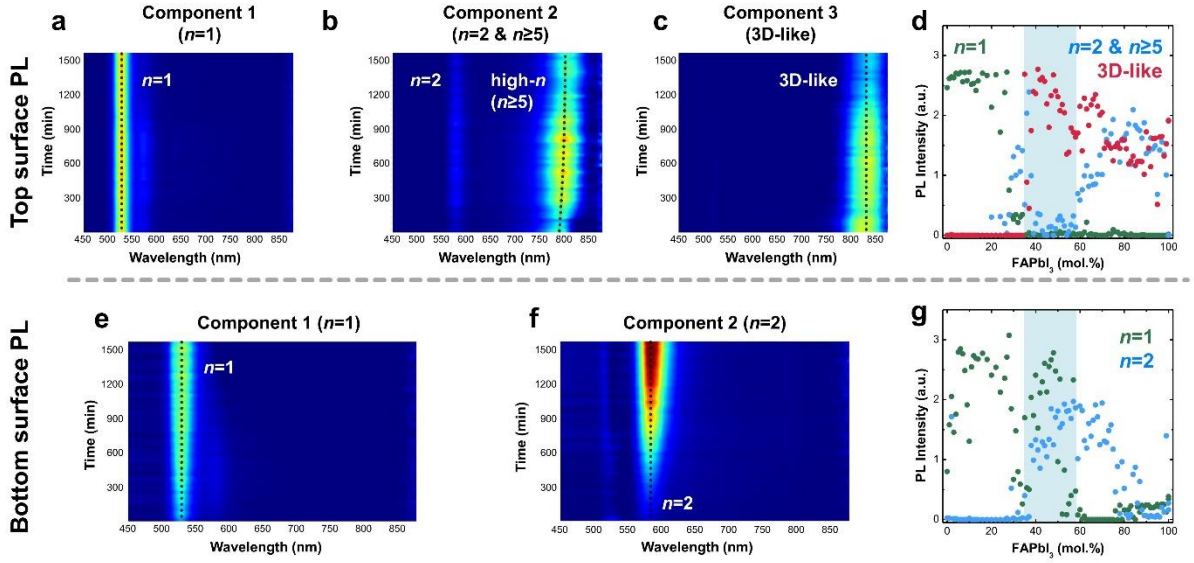

Fig. 2. a-c, NMF-deconvolution of time-evolved PL components of top surface PL spectra. **d**, Combined top-side PL loading maps of the corresponding components. **e** and **f**, NMF-deconvoluted time-evolved PL components of bottom surface PL spectra. **g**, Combined bottom-side PL loading maps of the corresponding components.

The time-evolved automated PL characterization creates a massive dataset of emission spectra (95 compositions in one cycle × 52 times for 26 hours (30 min interval) × top and bottom sides = 9880 individual PL spectra in total), which is impossible for human to manually analyze each spectrum. To effectively analyze the entire dataset and thereby gain quantitative insights into the emergence of different phases in the quasi-2D MHP compositional space, non-negative matrix factorization (NMF) – an unsupervised machine learning (ML)-based multivariate analysis – is applied to the overall PL dataset.[35] This is an effective method for separation of

multidimensional dataset to rapidly extract the key characteristics of PL evolution associated with the MHP phases, thereby revealing the overall phase distributions of the quasi-2D MHP system.

First, PL spectra of top surface were deconvoluted by three components as an optimal condition,[35] which are associated with the emission of n=1, n=2 and high-n (n≥5), and 3D-like MHP phases, respectively (**Fig. 2a-c**). The corresponding loading maps are combined in **Fig. 2d**, clearly revealing a distinctive phase-emerging regime for each PL component in the quasi-2D MHP compositional space. The n=1 phase exclusively emerges up to 20% $FAPbI_3$ ratio and then gradually disappears with increasing the ratio by 40%. Meanwhile, both n=2 and high-n phases, which are previously reported to emerge along with each other,[21] are dispersed into two regions in the 2D:3D compositional space: a sharp spike and hill at the $FAPbI_3$ ratio of 20-40% and >60%, respectively. Note that, by using four components for NMF deconvolution,[35] the n=2 phase is further separated out that only appears as a distinctive peak at the range of 20-40% $FAPbI_3$ ratio (**Supplementary Fig. 5**), indicating that high-n phases emerge at higher $FAPbI_3$ concentrations.[12, 16]

Interestingly, the 3D-like phase, with a PL peak centered at ~820 nm, start to emerge at ~35% $FAPbI_3$ ratio, showing a maximum PL intensity at the $FAPbI_3$ ratio of 40-50% where the PL emissions from other phases are insignificant in this composition range (a colored region in **Fig. 2d**). That is, the 3D-like phase is dominant at this range of $FAPbI_3$ ratio in the quasi-2D MHP compositional space, which is not consistent with the ideal MHP stoichiometry at this compositional range – corresponds with n=2 phase ($PEA_2FAPb_2I_7$). This can be attributed to the unbalanced crystallization kinetics between 2D, quasi-2D, and 3D-like phases, where the former can be more readily crystallized than 2D MHPs as observed in the previous study.[20] It is likely that the stronger interaction between spacer cation and polar solvent retards the crystallization of 2D MHP phases;[21, 24, 26] the high dipole moment of spacer cation compared to FA cation can ascribe this.[40] Note that the 3D-like phases have a structure where the crystal surface is passivated by 2D spacer cations protecting the MHP structure from external stresses, thereby manifesting better phase stability without compromising the excellent optoelectronic functionalities.[10, 38] In summary, the NMF analysis for top PL spectra provides a comprehensive understanding of how the phase distribution in quasi-2D MHP compositional space is regulated. Moreover, it reveals the optimal composition range which can be considered when designing these materials for desired functionalities.

Similarly, the bottom PL spectra are analyzed via NMF-deconvolution by two components, separating out the emission of n=1 and n=2 phases (i.e., PEA_2PbI_4 and $PEA_2FAPb_2I_7$) dispersed between 0-60 and 20-80% of $FAPbI_3$ ratios, respectively (**Fig. 2e-g**). There is a region where both 2D MHP phases appear together, qualitatively consistent with the region where the 3D-like phases appeared at the top surface. It is observed that both PL emissions become stronger over time of the measurements. This suggests slow but spontaneous crystallization kinetics of the 2D phases at room temperature – from the remaining 2D precursors after forming the 3D-like phase at the top surface.

The crystallization sequence and the resulting phase constitutions in the quasi-2D MHP films, particularly in the vertical direction, can be altered by the chemical nature of the substrate. The MHP films deposited onto the UV/O_3 treated glass substrates – a nominal thickness of ~800 nm confirmed by atomic force microscopy (**Supplementary Fig. 6**) – exhibit a similar PL trend at both top and bottom sides with negligible emission of n=2 phase (**Supplementary Fig. 7-9**). The mitigated vertical phase inhomogeneity could be attributed to the polar nature of the substrate after UV/O_3 treatment, which enhances solvent-substrate interaction and thereby release the spacer cations to participate in the overall crystallization process; Similar effect has been observed in quasi-2D MHP films incorporating polar precursors and/or ionic additives in the solutions.[41, 42] In addition, we note that the 3D-like phases start to emerge at lower $FAPbI_3$ ratios (~25%) and become dominant up to ~60%. Meanwhile, high-n phases develop in the similar compositional range observed from the MHP films formed onto the bare glass substrate (**Fig. 2b and d**), together with a very weak n=1 PL instead of that of the n=2 phase. From the observations, we hypothesize that the n=2 phase inhibits the emergence of 3D-like α-$FAPbI_3$ phase, consistent with the observations during the early-stage crystallization dynamics.[21] Except for the behavior of the n=2 phase, the overall phase distributions in the quasi-2D MHP compositional space are irrespective of the substrate. This provides essential understandings on how to achieve scalable fabrication of functional 3D-like MHP phases, while minimizing vertical phase inhomogeneity in spin-coating-free fabrication processes such as inkjet printing and blade coating.

Having understood the general tendency in phase distributions from PL, now we turn our focus onto the crystallographic structures of the quasi-2D MHP film system. To gain a comprehensive understanding of the crystal structures and orientation of the film system, HT-GIWAXS measurements are performed on all 96 MHP films in an array, giving high-

throughput insights into phase distributions and orientations in a 2D:3D compositional space (**Fig. 3a**). For measurements, three different incidence angles (φ) – 0.05 º, 0.1 º, and 0.5º – are employed, which provides more information of crystal structures and preferential orientation from the surface (first few nanometers) to the bulk (several hundred nanometers) of each film in an array with increasing the incidence angle (**Fig. 3b**).[43, 44]

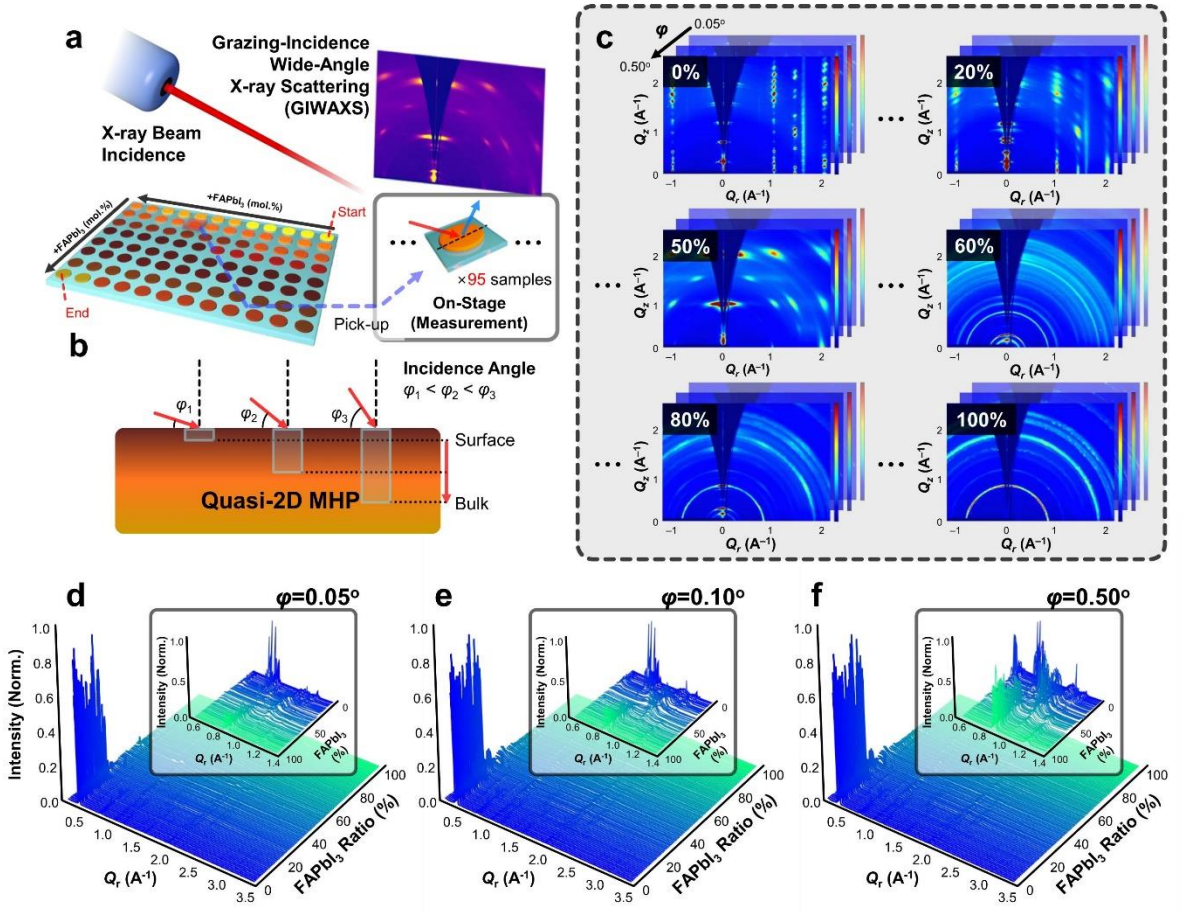

Fig. 3. a, Schematics of HT-GIWAXS characterization of the drop-casted quasi-2D MHP film array. **b**, Incidence angle dependence in GIWAXS patterns. With increasing the incidence angle, more information associated with the bulk is obtained. **c**, Representative GIWAXS 2D patterns of the films with different 2D:3D composition ratios collected via HT-GIWAXS at three different incidence angles (φ). **d-f**, 1D GIWAXS profiles of the MHP films at φ of 0.05, 0.1, and 0.5º, respectively. Insets in **d-f** display the magnified 1D profiles of the films at Q_r of 0.53-1.4 Å^{-1}, showing other MHP-related diffraction patterns such as α- and δ-$FAPbI_3$ phases.

For all φ, the overall 2D GIWAXS patterns show the global trend of phase transformation – along their preferential orientations – in the quasi-2D MHP film systems as a function of 2D:3D compositional ratio (**Fig. 3c** and **Supplementary Fig. S10-12**). Starting from the face-on oriented n=1 2D phase at 0% $FAPbI_3$, the face-on oriented n=2 phase emerges up to a $FAPbI_3$ ratio of 13%. Then the new vertically oriented crystallographic structure together with face-on oriented α-$FAPbI_3$ (100) phase (Q_r of ~1.02 $Å^{-1}$) starts to develop and dominates up to 55% $FAPbI_3$ ratio.[28, 38, 41] Such a vertically oriented 2D MHP structure is anticipated to render excellent charge conduction properties.[32] Recall that, however, the corresponding PL emissions of other 2D phases except for n=1 and 2 (specifically, n=3 and 4) were not observed in this system (**Fig. 1b and Supplementary Fig. 2**). Meanwhile, a ring-shaped pattern at Q_r = ~1.02 A^{-1} (random-oriented 3D α-$FAPbI_3$ phase) emerges from 42% $FAPbI_3$ ratio. Furthermore, the random-oriented δ-$FAPbI_3$ (a ring pattern at Q_r = ~0.86 $Å^{-1}$) phase emerges from ~50% $FAPbI_3$ and becomes distinctive with increasing ratio of $FAPbI_3$ to 100%. This is due to the thermodynamic stability of the non-perovskite phase at room temperature than the 3D MHP phase.[33] Note that there was a time interval between the fabrication of the film array and GIWAXS experiments, which manifests the α-to-δ phase transformation of the quasi-2D MHP films, particularly with high $FAPbI_3$ ratios.

To get quantitative insights into phase distributions in a 2D:3D compositional space, all the collected 2D GIWAXS patterns are converted to circular-averaged 1D profiles, giving 285 profiles in total (95 compositions × 3 different φ) as plotted in **Fig. 3d-f**. We first manually analyze the representative GIWAXS 1D profiles collected at φ=0.5° for key $FAPbI_3$ ratios (**Supplementary Fig. 13 and 14**). Evidently, there are noticeable changes of key diffraction peaks associated with the crystal structure of quasi-2D MHP phases (color-marked; **Supplementary Fig. 13b and 14b**), as a function of $FAPbI_3$ compositional ratios. Specifically, the GIWAXS analysis reveals the gradual change of α-$FAPbI_3$ phase orientations from vertically aligned direction to random orientation within the $FAPbI_3$ compositional range of 55-59%, which also involves the emergence of δ-$FAPbI_3$ phase (**Supplementary Fig. 14**). Overall, analyzing the entire 1D GIWAXS profiles can reveal a global trend of phase emergences in the quasi-2D MHP system with a quantitative sense.

However, practically, it requires tremendous effort and time for human to analyze all these profiles individually (**Supplementary Fig. 15**). To mitigate this challenge, we implemented an automated peak fitting function designed to trace the key diffraction peaks of quasi-2D MHP

systems in each 1D GIWAXS profile. This significantly accelerates the analysis time. In fact, it only takes 5 minutes to fully analyze a dataset of 96 profiles and therefore, it takes 15 minutes in total to complete phase identifications in the quasi-2D MHP compositional space at 3 different φ (**Fig. 4a**).

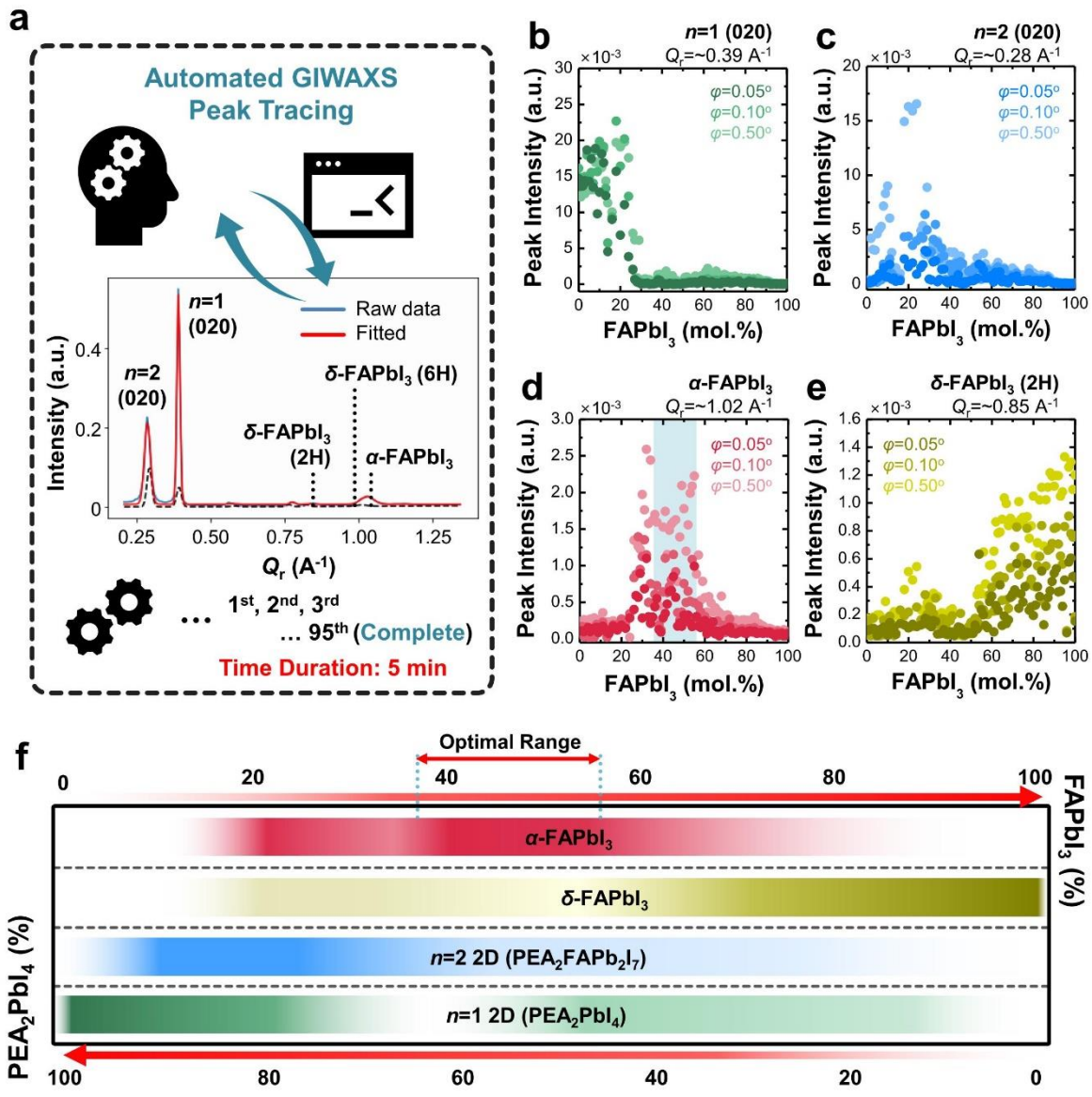

Fig. 4. a, A schematic describing automated GIWAXS peak analysis workflow. This accelerates the overall analysis sequences, thereby revealing the qualitative insights of the distribution of each phase as a function of the 2D:3D composition ratio within 5 min. **b-e**, GIWAXS peak intensities of n=1, n=2, α- and δ-$FAPbI_3$ phases as a function of 2D:3D composition ratio, respectively. **f**, The observed phase distributions in PEA-FA quasi-2D MHP film system.

Figs. 4b-e exhibit the distribution profiles of n=1, n=2, α-$FAPbI_3$, and δ-$FAPbI_3$ phases as a function of $FAPbI_3$ compositional ratio at each φ, respectively. Similar to the PL trend, the strong (020) GIWAXS peak of the n=1 phase (Q_r =~0.39 $Å^{-1}$) appears at lower $FAPbI_3$ concentrations, which becomes 10 to 100 times weaker for the $FAPbI_3$ ratios of over 25% (**Fig. 4b**). Within the low concentration of $FAPbI_3$ ratios, the peak intensity is irrespective of the φ, suggesting the n=1 2D phase is positioned at the top surface of the films. Note that, given the φ used for this study, the GIWAXS results only provide the crystallographic information about the first <1 μm from the foremost top of the film (thickness >4 μm); We cannot explore the crystal structure of the bottom side. The n=2 phase exhibits a strong (020) GIWAXS peak at the $FAPbI_3$ compositional range from 10-40% (**Fig. 4c**), which agrees with the trend seen in the PL spectra (**Fig. 2d**). This peak becomes stronger with increasing the φ, implying more n=2 MHP crystallites are formed in the film interior.

The GIWAXS intensity of the α-$FAPbI_3$ (100) phase shows double peaks at 20-40 and 40-60% $FAPbI_3$ ratios and becomes stronger with an increase of φ (**Fig. 4d**), where the compositional range of the latter region (color-marked) is consistent with that of the 3D-like phase in PL spectra. From the corresponding GIWAXS patterns collected at three φs, it is revealed that the α-$FAPbI_3$ (100) phase exhibits a face-on oriented alignment, as shown in the sharp Bragg spots in the 2D diffraction patterns (**Supplementary Fig. 10-14**). This indicates that the vertically aligned functional MHP structure can be extended to the film interior <1 μm, which is compatible with the actual device-level thickness. Given that the PL observations from the thin-film array where the distributions of the 3D-like phase is irrespective of the film thickness, the GIWAXS results suggest that the realization of highly oriented and stable α-$FAPbI_3$ that allows excellent vertical charge conduction is feasible, with some parametric optimizations in film fabrication process. There are weak signals of corner-sharing δ-$FAPbI_3$ phase (Q_r=0.99 $Å^{-1}$) at the $FAPbI_3$ compositional range of ~50-56% – around the upper bound of the range where the 3D-like phase is observed (**Supplementary Fig. 16**). This infers that the 3D-like phase can also undergo degradation at this range, which is, however, not much significant. Meanwhile, the GIWAXS intensity of the δ-$FAPbI_3$ phase – because of deformation of α-phase due to its thermodynamic instability – starts to emerge at a 60% $FAPbI_3$ ratio and gradually becomes stronger with further increasing the $FAPbI_3$ concentration (**Fig. 4e**). Overall, the observations from HT-GIWAXS characterizations clearly show a distinctive phase-emerging

region for each phase. The results also reveal that the stable, vertically oriented α-$FAPbI_3$ phase as a 3D-like MHP form can be exclusively formed at the $FAPbI_3$ compositional range of ~35-55% (**Fig. 4e**), consistent with the observation in PL analysis. These findings clearly provide quantitative evidence for uniting the spread notions regarding the optimal quasi-2D composition,[22, 24, 25, 45] which has no consensus to date – from its first photovoltaic applications.[46]

Recall that the phase distribution of the 3D-like MHP with excellent optoelectronic functionalities shows a similar trend when the thickness of the film is adjusted to the device-grade-thick level. This implies that our accelerated materials exploration strategy based on high-throughput material synthesis and characterization workflow provides fundamental insights and design principles that can be directly implemented into the scalable, mass-producible device manufacturing sequence. Subsequently, this will allow for accelerating the optimization process to realize efficient and stable solution-processable MHP optoelectronics on an industrial scale.

Outlook

In summary, the evolutions of phase emergences, distributions, and their stability assessments in the quasi-2D MHP films are systematically explored via high-throughput automated experimental workflow. From the analysis of high throughput PL spctroscopy, by implementing the unsupervised ML algorithm, both the compositional and geometric changes of MHP phase heterogeneities in the quasi-2D system are expeditiously quantified. This study not only facilitates the acceleration of materials exploration and discovery sequences but also provides comprehensive understanding of the complex quasi-2D system in an efficient manner. It is revealed that stable 3D-like α-$FAPbI_3$ MHP phases exclusively emerges at specific 2D:3D compositional range (35-55% of $FAPbI_3$ ratio). Ideally, this composition ratio corresponds with the n=2 2D MHP stoichiometry (at 50% $FAPbI_3$, $PEA_2FAPb_2I_7$), which is structurally not the case in this system. This suggests the desired functionalities in actual materials systems can appear far away from the expectations driven by conventional chemical knowledge based on stoichiometric calculations.

Comprehensive investigation of the crystallographic structures and orientations of the quasi-2D MHP systems is realized via HT-GIWAXS characterizations, where the integration of an

automated peak analysis function significantly accelerates the quantitative phase identifications within just 15 minutes. It is identified that the developed 3D-like phases observed in PL analysis indeed consist of α-$FAPbI_3$ MHPs with vertical orientation – advantageous to vertical charge conductions upon optoelectronic applications – and exhibits outstanding phase stability. In stark contrast, the quasi-2D MHPs with FA-rich compositions are readily transformed to the photo-inactive δ-phase, thereby failing the functionalities by time. Collectively, the high-throughput explorations of complex quasi-2D system uncover the optimal 2D:3D compositional ratios exhibiting the desired functionalities, thereby providing a generalized guideline for designing high-performance optoelectronics. In addition, our research reveals a crucial and all-encompassing principle that must be considered when designing phases of a material system. This principle can be readily applied in manufacturing processes that can be expanded without limitations.

Acknowledgements

J.Y. and M.A. acknowledge support from National Science Foundation (NSF), Award Number No. 2043205 and Alfred P. Sloan Foundation, award No. FG-2022-18275. J.H acknowledges the Department of Education Graduate Assistance in Areas of National Need (GAANN) program at Georgia Institute of Technology (Award #P200A180075). This research used the CMS 11-BM Beamline of the National Synchrotron Light Source II, a U.S. Department of Energy (DoE) Office Science User Facility operated for the DOE office of Science by Brookhaven National Laboratory under Contract DE-SC0012704. We sincerely appreciate Ruipeng Li for his contributions to HT-GIWAXS experiments.

Competing interests

The authors declare no competing interests.

References

1. Park, J.; Kim, J.; Yun, H. S.; Paik, M. J.; Noh, E.; Mun, H. J.; Kim, M. G.; Shin, T. J.; Seok, S. I., Controlled growth of perovskite layers with volatile alkylammonium chlorides.

Nature **2023**.

2. Jiang, Y.; Sun, C.; Xu, J.; Li, S.; Cui, M.; Fu, X.; Liu, Y.; Liu, Y.; Wan, H.; Wei, K.; Zhou, T.; Zhang, W.; Yang, Y.; Yang, J.; Qin, C.; Gao, S.; Pan, J.; Liu, Y.; Hoogland, S.; Sargent, E. H.; Chen, J.; Yuan, M., Synthesis-on-substrate of quantum dot solids. *Nature* **2022,** *612* (7941), 679-684.

3. Kim, J. S.; Heo, J. M.; Park, G. S.; Woo, S. J.; Cho, C.; Yun, H. J.; Kim, D. H.; Park, J.; Lee, S. C.; Park, S. H.; Yoon, E.; Greenham, N. C.; Lee, T. W., Ultra-bright, efficient and stable perovskite light-emitting diodes. *Nature* **2022,** *611* (7937), 688-694.

4. Ma, D.; Lin, K.; Dong, Y.; Choubisa, H.; Proppe, A. H.; Wu, D.; Wang, Y. K.; Chen, B.; Li, P.; Fan, J. Z.; Yuan, F.; Johnston, A.; Liu, Y.; Kang, Y.; Lu, Z. H.; Wei, Z.; Sargent, E. H., Distribution control enables efficient reduced-dimensional perovskite LEDs. *Nature* **2021,** *599* (7886), 594-598.

5. Zhang, H. T.; Park, T. J.; Zaluzhnyy, I. A.; Wang, Q.; Wadekar, S. N.; Manna, S.; Andrawis, R.; Sprau, P. O.; Sun, Y. F.; Zhang, Z.; Huang, C. Z.; Zhou, H.; Zhang, Z.; Narayanan, B.; Srinivasan, G.; Hua, N.; Nazaretski, E.; Huang, X. J.; Yan, H. F.; Ge, M. Y.; Chu, Y. S.; Cherukara, M. J.; Holt, M. V.; Krishnamurthy, M.; Shpyrko, O. G.; Sankaranarayanan, S. K. R. S.; Frano, A.; Roy, K.; Ramanathan, S., Perovskite neural trees. *Nature Communications* **2020,** *11* (1).

6. Kim, Y. H.; Park, J.; Kim, S.; Kim, J. S.; Xu, H.; Jeong, S. H.; Hu, B.; Lee, T. W., Exploiting the full advantages of colloidal perovskite nanocrystals for large-area efficient light-emitting diodes. *Nat Nanotechnol* **2022,** *17* (6), 590-597.

7. Duan, L.; Walter, D.; Chang, N.; Bullock, J.; Kang, D.; Phang, S. P.; Weber, K.; White, T.; Macdonald, D.; Catchpole, K.; Shen, H., Stability challenges for the commercialization of perovskite–silicon tandem solar cells. *Nat Rev Mater* **2023,** *8*, 261-281.

8. Meng, L.; You, J.; Yang, Y., Addressing the stability issue of perovskite solar cells for commercial applications. *Nat Commun* **2018,** *9*, 5265.

9. Boyd, C. C.; Cheacharoen, R.; Leijtens, T.; McGehee, M. D., Understanding Degradation Mechanisms and Improving Stability of Perovskite Photovoltaics. *Chem Rev* **2019,** *119* (5), 3418-3451.

10. Lee, J. W.; Dai, Z.; Han, T. H.; Choi, C.; Chang, S. Y.; Lee, S. J.; De Marco, N.; Zhao, H.; Sun, P.; Huang, Y.; Yang, Y., 2D perovskite stabilized phase-pure formamidinium perovskite solar cells. *Nat Commun* **2018,** *9* (1), 3021.

11. Li, X. T.; Hoffman, J. M.; Kanatzidis, M. G., The 2D Halide Perovskite Rulebook: How the Spacer Influences Everything from the Structure to Optoelectronic Device Efficiency.

Chemical Reviews **2021,** *121* (4), 2230-2291.

12. Soe, C. M. M.; Nagabhushana, G. P.; Shivaramaiah, R.; Tsai, H. H.; Nie, W. Y.; Blancon, J. C.; Melkonyan, F.; Cao, D. H.; Traore, B.; Pedesseau, L.; Kepenekian, M.; Katan, C.; Even, J.; Marks, T. J.; Navrotsky, A.; Mohite, A. D.; Stoumpos, C. C.; Kanatzidis, M. G., Structural and thermodynamic limits of layer thickness in 2D halide perovskites. *P Natl Acad Sci USA* **2019,** *116* (1), 58-66.

13. Lai, H.; Lu, D.; Xu, Z.; Zheng, N.; Xie, Z.; Liu, Y., Organic-Salt-Assisted Crystal Growth and Orientation of Quasi-2D Ruddlesden-Popper Perovskites for Solar Cells with Efficiency over 19. *Adv Mater* **2020,** *32* (33), 2001470.

14. Zhao, X. M.; Ball, M. L.; Kakekhani, A.; Liu, T. R.; Rappe, A. M.; Loo, Y. L., A charge transfer framework that describes supramolecular interactions governing structure and properties of 2D perovskites. *Nature Communications* **2022,** *13* (1).

15. Zhang, F.; Park, S. Y.; Yao, C.; Lu, H.; Dunfield, S. P.; Xiao, C.; Ulicna, S.; Zhao, X.; Du Hill, L.; Chen, X.; Wang, X.; Mundt, L. E.; Stone, K. H.; Schelhas, L. T.; Teeter, G.; Parkin, S.; Ratcliff, E. L.; Loo, Y. L.; Berry, J. J.; Beard, M. C.; Yan, Y.; Larson, B. W.; Zhu, K., Metastable Dion-Jacobson 2D structure enables efficient and stable perovskite solar cells. *Science* **2022,** *375* (6576), 71-76.

16. He, T.; Li, S.; Jiang, Y.; Qin, C.; Cui, M.; Qiao, L.; Xu, H.; Yang, J.; Long, R.; Wang, H.; Yuan, M., Reduced-dimensional perovskite photovoltaics with homogeneous energy landscape. *Nat Commun* **2020,** *11* (1), 1672.

17. Yang, J.; LaFollette, D. K.; Lawrie, B. J.; Ievlev, A. V.; Liu, Y.; Kelley, K. P.; Kalinin, S. V.; Correa-Baena, J. P.; Ahmadi, M., Understanding the Role of Cesium on Chemical Complexity in Methylammonium-Free Metal Halide Perovskites. *Adv Energy Mater* **2022**, 2202880.

18. Macpherson, S.; Doherty, T. A. S.; Winchester, A. J.; Kosar, S.; Johnstone, D. N.; Chiang, Y. H.; Galkowski, K.; Anaya, M.; Frohna, K.; Iqbal, A. N.; Nagane, S.; Roose, B.; Andaji-Garmaroudi, Z.; Orr, K. W. P.; Parker, J. E.; Midgley, P. A.; Dani, K. M.; Stranks, S. D., Local Nanoscale Phase Impurities are Degradation Sites in Halide Perovskites. *Nature* **2022**.

19. Chen, S.; Xiao, X.; Chen, B.; Kelly, L. L.; Zhao, J.; Lin, Y.; Toney, M. F.; Huang, J., Crystallization in one-step solution deposition of perovskite films: Upward or downward? *Sci Adv* **2021,** *7* (4), eabb2412.

20. Lin, Y.; Fang, Y.; Zhao, J.; Shao, Y.; Stuard, S. J.; Nahid, M. M.; Ade, H.; Wang, Q.; Shield, J. E.; Zhou, N.; Moran, A. M.; Huang, J., Unveiling the operation mechanism of layered perovskite solar cells. *Nat Commun* **2019,** *10* (1), 1008.

21. Yang, J.; Lawrie, B. J.; Kalinin, S. V.; Ahmadi, M., High-Throughput Automated Exploration of Phase Growth Kinetics in Quasi-2D Formamidinium Metal Halide Perovskites. *ChemRxiv* **2023**, chemrxiv-2023-bgcg0.

22. Zhang, Y.; Park, N. G., Quasi-Two-Dimensional Perovskite Solar Cells with Efficiency Exceeding 22%. *ACS Energy Lett* **2022,** *7*.

23. Wang, K.; Lin, Z. Y.; Zhang, Z.; Jin, L.; Ma, K.; Coffey, A. H.; Atapattu, H. R.; Gao, Y.; Park, J. Y.; Wei, Z.; Finkenauer, B. P.; Zhu, C.; Meng, X.; Chowdhury, S. N.; Chen, Z.; Terlier, T.; Do, T. H.; Yao, Y.; Graham, K. R.; Boltasseva, A.; Guo, T. F.; Huang, L.; Gao, H.; Savoie, B. M.; Dou, L., Suppressing phase disproportionation in quasi-2D perovskite light-emitting diodes. *Nat Commun* **2023,** *14* (1), 397.

24. Caiazzo, A.; Janssen, R. A. J., High Efficiency Quasi-2D Ruddlesden–Popper Perovskite Solar Cells. *Adv Energy Mater* **2022,** *12*, 2202830.

25. Coffey, A. H.; Yang, S. J.; Gomez, m.; Finkenauer, B. P.; Terlier, T.; Zhu, C.; Dou, L., Controlling Crystallization of Quasi-2D Perovskite Solar Cells: Incorporating Bulky Conjugated Ligands. *Adv Energy Mater* **2022**, 2201501.

26. Zhang, X.; Munir, R.; Xu, Z.; Liu, Y.; Tsai, H.; Nie, W.; Li, J.; Niu, T.; Smilgies, D. M.; Kanatzidis, M. G.; Mohite, A. D.; Zhao, K.; Amassian, A.; Liu, S. F., Phase Transition Control for High Performance Ruddlesden-Popper Perovskite Solar Cells. *Adv Mater* **2018,** *30* (21), e1707166.

27. Soe, C. M. M.; Nie, W. Y.; Stoumpos, C. C.; Tsai, H.; Blancon, J. C.; Liu, F. Z.; Even, J.; Marks, T. J.; Mohite, A. D.; Kanatzidis, M. G., Understanding Film Formation Morphology and Orientation in High Member 2D Ruddlesden-Popper Perovskites for High-Efficiency Solar Cells. *Advanced Energy Materials* **2018,** *8* (1).

28. Zhou, N.; Shen, Y.; Li, L.; Tan, S.; Liu, N.; Zheng, G.; Chen, Q.; Zhou, H., Exploration of Crystallization Kinetics in Quasi Two-Dimensional Perovskite and High Performance Solar Cells. *J Am Chem Soc* **2018,** *140* (1), 459-465.

29. Sun, C.; Jiang, Y.; Cui, M.; Qiao, L.; Wei, J.; Huang, Y.; Zhang, L.; He, T.; Li, S.; Hsu, H. Y.; Qin, C.; Long, R.; Yuan, M., High-performance large-area quasi-2D perovskite light-emitting diodes. *Nat Commun* **2021,** *12* (1), 2207.

30. Quan, L.; Ma, D. X.; Zhao, Y. B.; Voznyy, O.; Yuan, H. F.; Bladt, E.; Pan, J.; de Arquer, F. P. G.; Sabatini, R.; Piontkowski, Z.; Emwas, A. H.; Todorovic, P.; Quintero-Bermudez, R.; Walters, G.; Fan, J. Z.; Liu, M. X.; Tan, H. R.; Saidaminov, M. I.; Gao, L.; Li, Y. Y.; Anjum, D. H.; Wei, N. N.; Tang, J.; McCamant, D. W.; Roeffaers, M. B. J.; Bals, S.; Hofkens, J.; Bakr, O. M.; Lu, Z. H.; Sargent, E. H., Edge stabilization in reduced-dimensional perovskites. *Nature Communications* **2020,** *11* (1).

31. Sanchez, S. L.; Yang, J.; Ahmadi, M., Understanding the Ligand-Assisted Reprecipitation of CsPbBr3 Perovskite Nanocrystals via High Throughput Robotic Synthesis Approach. *ChemRxiv* **2023**, 10.26434/chemrxiv-2023-bgcg0.

32. Yan, L.; Ma, J.; Li, P.; Zang, S.; Han, L.; Zhang, Y.; Song, Y., Charge-Carrier Transport in Quasi-2D Ruddlesden-Popper Perovskite Solar Cells. *Adv Mater* **2022,** *34* (7), e2106822.

33. Pool, V. L.; Dou, B.; Van Campen, D. G.; Klein-Stockert, T. R.; Barnes, F. S.; Shaheen, S. E.; Ahmad, M. I.; van Hest, M. F.; Toney, M. F., Thermal engineering of FAPbI3 perovskite material via radiative thermal annealing and in situ XRD. *Nat Commun* **2017,** *8*, 14075.

34. Higgins, K.; Valleti, S. M.; Ziatdinov, M.; Kalinin, S. V.; Ahmadi, M., Chemical Robotics Enabled Exploration of Stability in Multicomponent Lead Halide Perovskites via Machine Learning. *Acs Energy Letters* **2020,** *5* (11), 3426-3436.

35. Higgins, K.; Ziatdinov, M.; Kalinin, S. V.; Ahmadi, M., High-Throughput Study of Antisolvents on the Stability of Multicomponent Metal Halide Perovskites through Robotics-Based Synthesis and Machine Learning Approaches. *J Am Chem Soc* **2021,** *143* (47), 19945-19955.

36. Zhang, J.; Langner, S.; Wu, J.; Kupfer, C.; Luer, L.; Meng, W.; Zhao, B.; Liu, C.; Daum, M.; Osvet, A.; Li, N.; Halik, M.; Stubhan, T.; Zhao, Y.; Hauch, J.; Brabec, C. J., Intercalating-Organic-Cation-Induced Stability Bowing in Quasi-2D Metal-Halide Perovskites. *ACS Energy Letters* **2022,** *7*, 70-77.

37. Zhang, J.; Wu, J.; Langner, S.; Zhao, B.; Xie, Z.; Hauch, J. A.; Afify, H. A.; Barabash, A.; Luo, J.; Sytnyk, M.; Meng, W.; Zhang, K.; Liu, C.; Osvet, A.; Li, N.; Halik, M.; Heiss, W.; Zhao, Y.; Brabec, C. J., Exploring the Steric Hindrance of Alkylammonium Cations in the Structural Reconfiguration of Quasi-2D Perovskite Materials Using a High-throughput Experimental Platform. *Adv Funct Mater* **2022**, 2207101.

38. Chen, A. Z.; Shiu, M.; Ma, J. H.; Alpert, M. R.; Zhang, D.; Foley, B. J.; Smilgies, D. M.; Lee, S. H.; Choi, J. J., Origin of vertical orientation in two-dimensional metal halide perovskites and its effect on photovoltaic performance. *Nat Commun* **2018,** *9* (1), 1336.

39. Ma, F.; Li, J.; Li, W.; Lin, N.; Wang, L.; Qiao, J., Stable α/δ phase junction of formamidinium lead iodide perovskites for enhanced near-infrared emission. *Chem Sci* **2017,** *8* (1), 800-805.

40. Song, H.; Yang, J.; Jeong, W. H.; Lee, J.; Lee, T. H.; Yoon, J. W.; Lee, H.; Ramadan, A. J.; Oliver, R. D. J.; Cho, S. C.; Lim, S. G.; Jang, J. W.; Yu, Z.; Oh, J. T.; Jung, E. D.; Song, M. H.; Park, S. H.; Durrant, J. R.; Snaith, H. J.; Lee, S. U.; Lee, B. R.; Choi, H., A Universal Perovskite Nanocrystal Ink for High-Performance Optoelectronic Devices. *Adv Mater* **2023,** *35*, 2209486.

41. Liang, C.; Gu, H.; Xia, Y. D.; Wang, Z.; Liu, X. T.; Xia, J. M.; Zuo, S. W.; Hu, Y.; Gao, X. Y.; Hui, W.; Chao, L. F.; Niu, T. T.; Fang, M.; Lu, H.; Dong, H.; Yu, H.; Chen, S.; Ran, X. Q.; Song, L.; Li, B. X.; Zhang, J.; Peng, Y.; Shao, G. S.; Wang, J. P.; Chen, Y. H.; Xing, G. C.; Huang, W., Two-dimensional Ruddlesden-Popper layered perovskite solar cells based on phase-pure thin films. *Nature Energy* **2021,** *6* (1), 38-+.

42. Yang, J.; He, T.; Li, M.; Li, G.; Xu, J.; Zhang, M.; Zuo, W.; Qin, R.; Aldamasy, M. H.; Yuan, M.; Li, Z.; Byranvand, M. M.; Saliba, M.; Abate, A., π-Conjugated Carbazole Cations Enable Wet-Stable Quasi-2D Perovskite Photovoltaics. *ACS Energy Lett* **2022,** *7*, 4451-4458.

43. Perini, C. A. R.; Rojas-Gatjens, E.; Ravello, M.; Castro-Mendez, A. F.; Hidalgo, J.; An, Y.; Kim, S.; Lai, B.; Li, R.; Silva-Acuna, C.; Correa-Baena, J. P., Interface Reconstruction from Ruddlesden-Popper Structures Impacts Stability in Lead Halide Perovskite Solar Cells. *Adv Mater* **2022,** *34* (51), e2204726.

44. Hidalgo, J.; Perini, C. A. R.; Castro-Mendez, A. F.; Jones, D.; Kobler, H.; Lai, B.; Li, R. P.; Sun, S. J.; Abate, A.; Correa-Baena, J. P., Moisture-Induced Crystallographic Reorientations and Effects on Charge Carrier Extraction in Metal Halide Perovskite Solar Cells. *Acs Energy Letters* **2020,** *5* (11), 3526-3534.

45. Liang, J.; Zhang, Z.; Xue, Q.; Zheng, Y.; Wu, X.; Huang, Y.; Wang, X.; Qin, C.; Chen, Z.; Chen, C. C., A finely regulated quantum well structure in quasi-2D Ruddlesden–Popper perovskite solar cells with efficiency exceeding 20%. *Energy Environ Sci* **2022,** *15*, 296-310.

46. Smith, I. C.; Hoke, E. T.; Solis-Ibarra, D.; McGehee, M. D.; Karunadasa, H. I., A layered hybrid perovskite solar-cell absorber with enhanced moisture stability. *Angew Chem Int Ed Engl* **2014,** *53* (42), 11232-5.